

## Ligand-Induced Conformational Changes in Poliovirus–Antiviral Drug Complexes

CHAITANYA N. HIREMATH,<sup>a</sup> DAVID J. FILMAN,<sup>a</sup> ROBERT A. GRANT<sup>a</sup> AND JAMES M. HOGLE<sup>a,b,\*</sup>

<sup>a</sup>Department of Biological Chemistry and Molecular Pharmacology, Harvard Medical School, Boston, MA 02115, USA, and <sup>b</sup>Committee on Higher Degrees in Biophysics, Harvard University, Cambridge, MA 02138, USA. E-mail: hogle@hogles.med.harvard.edu

(Received 25 October 1996; accepted 12 February 1997)

### Abstract

Crystal structures of the Mahoney strain of type 1 poliovirus complexed with the antiviral compounds R80633 and R77975 were determined at 2.9 Å resolution. These compounds block infection by preventing conformational changes required for viral uncoating. In various drug–poliovirus complexes reported earlier, no significant conformational changes were found in the structures of the capsid proteins. In the structures reported here, the strain of virus is relatively insensitive to these antivirals. Correspondingly, significant conformational changes are necessary to accommodate the drug. These conformational changes affect both the immediate vicinity of the drug binding site, and more distant loops located near the fivefold axis. In addition, small but concerted shifts of the centers of mass of the major capsid proteins consistently have been detected whose magnitudes are correlated inversely with the effectiveness of the drugs. Collectively, the drug complexes appear to sample the conformational repertoire of poliovirus near equilibrium, and thus provide a possible model for the earliest stages of viral uncoating during infection.

### 1. Introduction

The picornaviruses are a family of small non-enveloped viruses whose members include polio-, rhino-, foot-and-mouth disease, coxsackie-, cardio- and hepatitis A viruses. The protein shell of each virion encapsidates one copy of a single-stranded plus-sense RNA genome. This protein shell is composed of 60 copies each of four capsid proteins, VP1, VP2, VP3 and VP4, arranged on an icosahedral lattice. The three large capsid proteins share a common core structural motif, an eight-stranded antiparallel  $\beta$ -barrel.

In the crystal structures of poliovirions (Hogle, Chow & Filman, 1985; Filman *et al.*, 1989), the hydrophobic core of the  $\beta$ -barrel of major capsid protein VP1 invariably is occupied by a long-chain hydrocarbon ligand, or mixture of such ligands. Depending on their appearance, these natural ligands have been modeled as sphingosine (Filman *et al.*, 1989), palmitate (Yeates *et al.*, 1991), or laurate (Jacobson, 1995). Some strains of the closely related rhinoviruses (Kim *et al.*, 1989; Oliveira *et al.*,

1993), as well as bovine enterovirus (Smyth *et al.*, 1995), and coxsackievirus B3 (Muckelbauer *et al.*, 1995) have been reported to contain shorter-chain fatty acids in the analogous lipid-binding site. The natural ligand is believed to play an important role in modulating the thermal stability of these picornaviruses, possibly regulating viral assembly and cell entry (Filman *et al.*, 1989; Flore, Fricks, Filman & Hogle, 1990).

When poliovirus, or a closely related virus, binds to its specific host-cell receptor at physiologic temperature, it undergoes a series of extensive conformational changes which result in the externalization and/or release of internal components of the protein shell. First, the release of the myristoylated internal peptide, VP4, and the externalization of the amino terminus of VP1 produce the 135S particle, which is suspected to be an intermediate in infection (Fricks & Hogle, 1990). Later, the release of viral RNA produces the 80S empty capsid (Roizman, Mayer & Roane, 1959). Formation of both 135S and 80S particles is suspected to involve concerted movement of the capsid proteins, requiring most or all 60 copies of each protein to undergo similar conformational changes.

Several antiviral compounds are known to prevent this uncoating process and to stabilize the virus against thermal inactivation (McSharry, Caligui & Eggers, 1979; Andries *et al.*, 1990). The crystal structures of several virus–antiviral drug complexes have been reported for both polioviruses and human rhinoviruses (Smith *et al.*, 1986; Badger *et al.*, 1988; Badger, Minor, Oliveira, Smith & Rossmann, 1989; Kim *et al.*, 1993; Oliveira *et al.*, 1993; Grant *et al.*, 1994; Hiremath, Grant, Filman & Hogle, 1995). The antiviral compounds are generally elongated molecules, similar in length to the natural ligands of poliovirus. These molecules all bind in a slightly bent conformation in the same site as the natural ligand. In human rhinovirus 14, where the natural ligand is absent from the native virus, large conformational differences were seen upon drug binding, primarily in the immediate vicinity of the drug binding pocket (Smith *et al.*, 1986; Badger *et al.*, 1988, 1989). However, in polioviruses and in rhinovirus strains whose native structures contain a bound ligand, the drug-bound structures were much more similar to the native structures containing the natural ligand (Kim *et al.*, 1989; Oliveira *et al.*, 1993; Grant *et al.*, 1994).

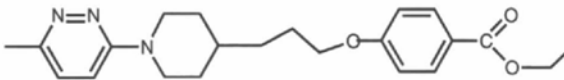
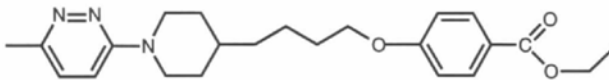
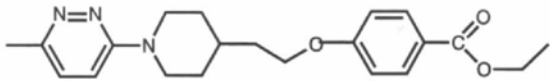
	MIC ( $\mu\text{M}$ )	
	P1/Mahoney	P3/Sabin
R78206 	0.008	0.005
R80633 	0.511	0.013
R77975 	3.061	0.206

Fig. 1. The structures of three antiviral compounds from Janssen Pharmaceutica. The values alongside each structure indicate the minimum inhibitory concentration of that compound required for the inhibition of the P1/Mahoney and P3/Sabin strains of poliovirus.

A previous publication from this laboratory (Grant *et al.*, 1994) described crystal structures of the Sabin vaccine strain of type 3 poliovirus (P3/Sabin) in complex with a series of antiviral compounds from Janssen Pharmaceutica: R78206, R80633 and R77975, and with WIN51711 from Sterling-Winthrop. Of these compounds, R78206 was the most effective, with the lowest minimum inhibitory concentration (MIC), and R77975 was the least effective (Fig. 1). Complexes with R78206 were also reported for P1/Mahoney, a neurovirulent laboratory strain of type 1 poliovirus, and for P3/242-H2, a double mutant of P3/Sabin with an elevated sensitivity to the drug. Drug binding caused no significant conformational changes remote from the immediate binding site in any of those structures.

Grant *et al.* concluded that the efficacy of the compounds was related to their ability to fill the available space within the pocket without causing steric conflicts that would disrupt the normal structure of the capsid. This complementarity between the drug and the binding site is related to the size, shape and flexibility of the drug, as well as the sequence and side-chain conformations of the amino acids lining the binding site. A few specific side chains play critical roles. Modeling experiments suggested that the binding of the either R80633 or R77975 to P1/Mahoney would cause significant steric conflicts. It was suggested that these conflicts were responsible for the significantly lower sensitivity of P1/Mahoney to these compounds, compared with P3/Sabin.

The present paper reports the crystal structures for the Mahoney strain of type 1 poliovirus complexed with the antiviral drugs R80633 and R77975. Consistent with the predictions of Grant *et al.*, the complexes with these lower affinity drugs display significantly larger structural changes in the drug binding pocket. Moreover, for the

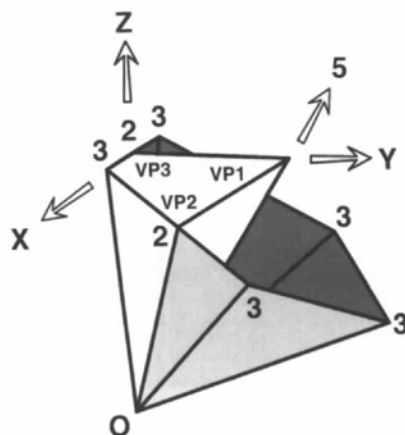


Fig. 2. How the X, Y and Z directions are defined in the vicinity of the standard protomer. The X, Y and Z axes are mutually orthogonal icosahedral twofold axes, passing through the center of the virus (which is labeled O). In this perspective drawing, the protomer chosen to be the standard one is shown, with the positions of the major capsid proteins, VP1, VP2, and VP3 indicated. The Z axis (the arrow labeled Z) increases radially outward from the center of the virus (labeled O). This axis is one of two icosahedral twofolds (labeled 2) that delimit the standard protomer. The arrow labeled X lies parallel to the X axis. In the vicinity of the standard protomer, the X direction increases when going away from the Z axis towards one of the adjacent threefold axes (labeled 3). The arrow labeled Y lies parallel to the Y axis. In the vicinity of the standard protomer, the Y direction increases when going away from the Z axis towards the adjacent fivefold axis (labeled 5). Collectively, the five threefold axes shown here define the geometric limits of a pentamer.

first time in poliovirus, significant structural changes are seen distant from the drug binding pocket. These changes include alterations in the structures of polypeptide loops of VP1 located near the particle fivefold axis of the R80633 complex, and to a lesser extent, the R77975 complex.

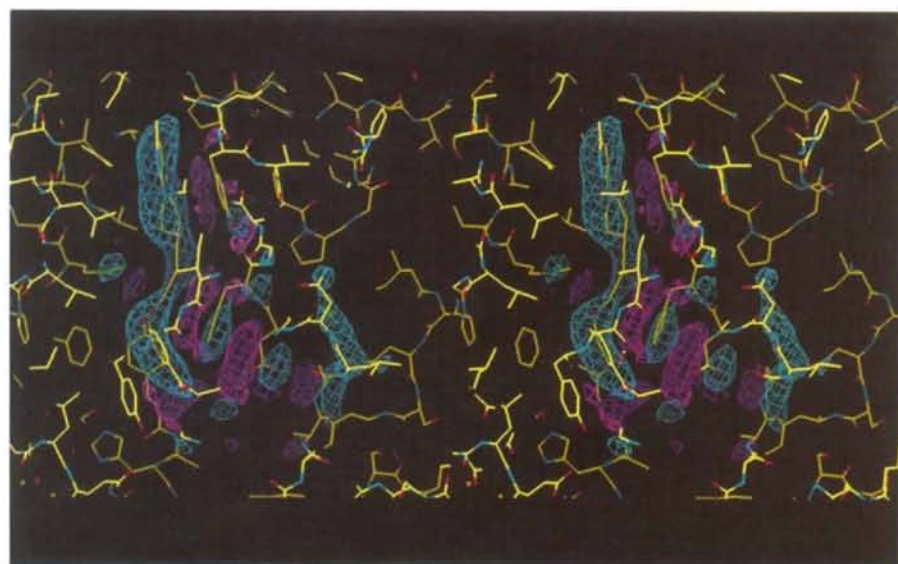
There is an accumulating database of independently refined poliovirus crystal structures, with a variety of different antiviral compounds bound, and including a number of poliovirus sequences. This database has now revealed some surprisingly accurate quantitative relationships between capsid structure and drug effectiveness. The binding of various antiviral compounds to poliovirus apparently causes small but reproducible concerted changes in the positions of the capsid proteins. Most strikingly, the measured effectiveness of each antiviral compound has a strong inverse correlation with the magnitude of the changes its binding causes in the structure of the capsid. These comparisons suggest how

local changes caused by the binding of certain antiviral compounds are propagated through the virus, and might thereby affect the stability of these complexes. They provide insights into the dynamic repertoire of the virus, and may lead to an improved understanding of the uncoating process during infection.

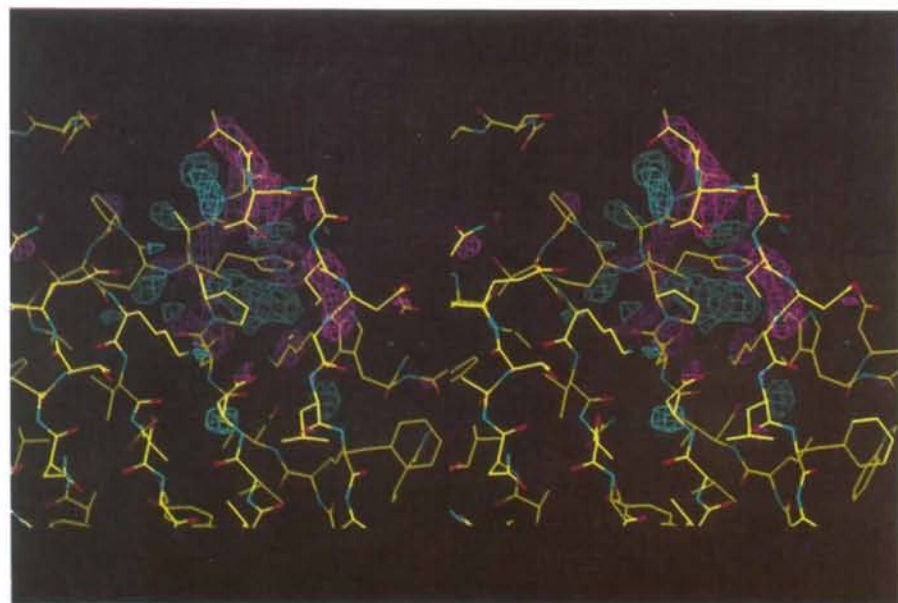
## 2. Methods

### 2.1. Virus propagation and crystallization

P1/Mahoney was prepared from a low-passage stock, generously provided by Marie Chow, of a plaque isolated from HeLa cells transfected with an infectious



(a)



(b)

Fig. 3. The largest difference density features in the R80633 complex with P1/Mahoney. In these stereo representations, atoms are colored by type: C atoms are yellow, N atoms are cyan, O atoms are red, and S atoms are green. Positive difference features are blue and negative features are red. These contours are at 4.0 standard deviations from the mean. (a) The lipid binding pocket and its immediate vicinity. The presence and orientation of the drug is indicated by a strong positive difference feature. Binding of this drug causes correlated movements in the carboxyl end of the GH loop of VP1 (right), and in the side chain of Met1132 (left). (b) Concerted shifts are seen in the BC, HI, and DE loops of VP1, which are located near the fivefold axis, distant from the drug binding site.

cDNA clone of the viral genome (Racaniello & Baltimore, 1981). The virus was grown in HeLa cells and purified by differential centrifugation and CsCl density-gradient fractionation (Baltimore, Girard & Darnell, 1966) and crystallized by microdialysis *versus* low ionic strength. The crystals of P1/Mahoney belong to space group  $P2_12_12_1$ , with  $a = 322.9$ ,  $b = 358.0$ , and  $c = 380.2$  Å, and contain 1/2 virus particle per asymmetric unit. Prior to use, crystals grown in dialysis buttons were equilibrated *versus* a synthetic mother liquor containing 25%(v/v) ethylene glycol in PMC7 buffer (10 mM NaPIPES, 5 mM MgCl<sub>2</sub>, 1 mM CaCl<sub>2</sub>, pH 7.0).

## 2.2. Preparation of virus–drug complexes

The antiviral drugs R80633 and R77975 (Fig. 1) were obtained from K. Andries at Janssen Pharmaceutica. Solid drug was dissolved in dimethyl sulfoxide (DMSO) at 10 mg ml<sup>-1</sup> and stored at 193 K until use. Saturated solutions of drugs in the synthetic mother liquor were prepared by adding the stock solution until the mixture turned turbid, and then clearing undissolved material by centrifugation for 10 min in an Eppendorf microcentrifuge. The final concentration of DMSO was approximately 4%. Freshly grown crystals of the native virus were soaked in freshly prepared saturated solutions of drug at 277 K for at least a week. Because crystals were damaged by direct transfer to saturated solutions of R77975, crystals were first equilibrated with a 50% saturated solution for a few days before transfer to the higher concentration.

## 2.3. Data collection and processing

The crystals were mounted in sealed capillary tubes for data collection. Three-dimensional diffraction data were collected at 261 K by oscillation photography using

Cu K $\alpha$  radiation from an Enraf–Nonius GX-13 rotating-anode generator with a 100  $\mu$ m focus and Franks mirror optics. 0.5° oscillation photographs were obtained from 3–4 h exposures. The films were digitized, integrated and processed as described previously (Yeates *et al.*, 1991; D. J. Filman, unpublished work). Films were scaled and post-refined (Winkler, Schutt & Harrison, 1979) using the Fourier transform of the icosahedrally constrained electron-density map of the native structure as a reference. Three-dimensional data sets were assembled from multiple films and included measurements of partially recorded reflections (50% partial or greater) after correction to their fully recorded equivalents. Following the initial post-refinement, films were routinely re-integrated and re-processed to exploit the improved knowledge of crystal orientation parameters.

## 2.4. Difference maps

Drug-minus-native difference Fourier coefficients,  $(|F_{\text{drug}}| - |F_{\text{native}}|)\exp(i\varphi_{\text{native}})$ , were constructed using observed structure-factor magnitudes from the virus–drug complex, together with amplitudes and phases from the native structure. These coefficients were Fourier transformed and the resulting electron-density map was averaged. Structure factors for the native P1/Mahoney structure represent the Fourier transform of an icosahedrally constrained electron-density map after convergence of the (30-fold) non-crystallographic symmetry (NCS) based phase constraint procedure, using a local implementation of the method of Bricogne (Bricogne, 1974).

## 2.5. Refinement of models and phases

Atomic models for the virus and the drug were built to fit icosahedrally constrained ' $F_o$ ' maps using



Fig. 4. Stereo ribbon representation of the P1/Mahoney poliovirus protomer showing the location of loops in VP1 that are modified by the binding of R80633. The GH loop is dark purple. The BC, HI and DE loops, located near the fivefold axis, are yellow, red, and green, respectively. The remainder of the main chain is shown in light magenta as a continuous ribbon. The dark blue surface represents the location of bound drug.

the graphics program *FRODO* (Jones, 1978) and refined by pseudo-real-space methods (Jacobson, Hogle & Filman, 1996). For efficiency, this refinement was limited to the protomer box, a somewhat arbitrary box-shaped portion of the asymmetric unit large enough to enclose one chemically continuous poliovirus protomer, plus its immediate neighborhood. The crystallographic component of the refinement residual was calculated based on the pretense that this small pseudo-cell was periodic. Thus, Fourier transformation of averaged electron density yielded complex-valued pseudo-structure-factor standards whose reference phases remain unchanged during refinement of the model.

Further improvements in the phases were obtained by re-initiating NCS-based phase refinement using the latest partially refined atomic model as a source of molecular replacement phases. Similarly, further improvement of the atomic models was achieved by re-refining the model, using the most recent averaged ' $F_o$ ' map as a standard. The final refined structure was obtained by alternating these two procedures until convergence.

#### 2.6. Estimation of drug occupancy

Estimating the occupancy of the bound drug molecule (Smith *et al.*, 1986; Grant *et al.*, 1994) requires knowing both the fraction of binding sites that are vacant, and the proportion of occupied sites that contain drug, rather than natural ligand. In the protomer-box-based refinement of the atomic model, the optimized drug-molecule occupancy provided an estimate of the fraction of occupied sites (here about 100%). The ratio between ligands then was obtained from a second calculation. One set of model-based pseudo-structure factors was calculated from an atomic model of the native poliovirus structure, and another set was calculated from a model of the drug-virus complex. Whichever linear combination of these two sets agreed best with the transform of the reference protomer box map (in a least-squares sense) indicated the relative proportions of natural ligand and drug in the crystal structure.

#### 2.7. Calculation of $\beta$ -barrel shifts

Calculations were performed to establish whether the binding of antiviral drugs caused concerted shifts in the major capsid proteins, VP1, VP2, and VP3, and whether these shifts were correlated with drug effectiveness. For each protein, shifts in the center of mass were determined by comparing the coordinates from two independently refined atomic models. Similar results were usually obtained from  $C\alpha$  models, main-chain models, complete atomic models, or main-chain models limited to the  $\beta$ -barrels of the capsid proteins.

To determine the vector direction of the shift, the  $X$ ,  $Y$  and  $Z$  components were plotted separately for each protein. The  $X$ ,  $Y$  and  $Z$  directions represent three mutually perpendicular twofold axes of the icosahedral

virus particle. In the vicinity of the standard protomer upon which the calculation is based (Fig. 2), the  $Z$  direction represents a shift radially outward from the center of the virus, along a particular icosahedral twofold axis; the  $X$  direction represents a shift perpendicular to the  $Z$  direction away from the twofold axis, towards a neighboring threefold; and the  $Y$  direction is perpendicular to  $X$  and  $Z$ , and represents a shift from the twofold toward a neighboring fivefold. The  $X$ ,  $Y$ , and  $Z$  shifts in symmetry-related protomers can be obtained by applying standard icosahedral operators to the shifts listed here.

#### 2.8. Correlating shifts with drug effects

Scatter plots were produced to correlate the biological effects of the drugs with the magnitude and direction of the shift caused by drug binding in each of the major capsid proteins. Each plotted point represents a specific drug in a particular strain of virus. In these plots, the abscissa represents the biological effect, showing the natural logarithm of the MIC. MIC values for particular drugs in specific strains of poliovirus were determined by K. Andries (Janssen Research Foundation, Belgium) and reported in Grant *et al.* (1994). Distances along the ordinate represent the difference in coordinates between two independently refined atomic models. 'Drug-complex-minus-native' coordinate comparisons were made for the binding of R78206, R80633, and R77975 to P1/Mahoney; for binding of R78206, R80633 and R77975 and WIN51711 to P3/Sabin; and for the binding of R78206 to P3/242-H2, a double mutant of P3/Sabin which is particularly susceptible to the drugs. The coordinate sets used for these comparisons include every drug-poliovirus complex thus far determined: all six drug-poliovirus complexes reported previously (Grant *et al.*, 1994; Hiremath *et al.*, 1995) and both of the complexes reported in the present paper. For the native structures, the refined coordinates of P3/Sabin (Filman *et al.*, 1989; Syed, Filman & Hogle unpublished work), P1/Mahoney (Jacobson *et al.*, 1996) and P3/242-H2 (Syed, Filman & Hogle, unpublished work) were used.

### 3. Results

#### 3.1. Structure determination

3.1.1. *Diffraction data.* Statistics for the three-dimensional X-ray diffraction data are shown in Table 1. The final data sets are only partially complete but are adequately over-sampled because of the 30-fold non-crystallographic symmetry. The merging statistics are comparable with those observed for native poliovirus crystals.

3.1.2. *Difference map.* An icosahedrally averaged  $F_{\text{drug}} - F_{\text{native}}$  difference electron-density map, with phases based on the icosahedrally constrained native structure, was used to locate differences in the structure of the protein capsid (Fig. 3). As seen previously,

Table 1. *Data statistics*

	R80633	R77975
Number of crystals used	3	7
Number of films collected	20	16
Number of measurements collected	730623	587697
Number of unique <i>hkl</i>	419439	306408
Number of unique <i>hkl</i> used*	343453	237778
Maximum resolution (Å)	2.9	2.9
Completeness of data (%)	35	24
$R_{\text{merge}}^{\dagger}$ (all measurements > 50% partial)	0.160	0.148
$R_{\text{merge}}^{\dagger}$ (fully recorded reflections only)	0.127	0.115

\*Partially recorded measurements less than 50% partial were rejected, together with <1% of measurements with very poor  $I/\sigma$  values. The  $I/\sigma$  cut used here does not specifically eliminate weak measurements. Instead, it eliminates those reflections whose large fractional errors indicate problems in integration (e.g. due to severe overlaps or saturated pixels).  $\dagger R_{\text{merge}} = \sum_{hj} |I_{hj} - \langle I_h \rangle| / \sum_{hj} I_{hj}$ , where  $\langle I_h \rangle$  represents the statistically weighted mean of individual intensity measurements,  $I_{hj}$ .

significant difference features were observed in the lipid binding pocket of VP1. Differences also were observed in the entrance to the pocket, in residues 1232–1238 from the *GH* loop of VP1. Most unexpectedly, changes were also seen quite distant from the drug binding site, in loops of VP1 located near the particle fivefold axis (see Fig. 4). These differences occurred in the vicinity of the *BC* loop (residues 1096–1102), the *DE* loop (residues 1142–1152) and the *HI* loop (residues 1245–1251). A more detailed description follows below.

3.1.3. *Molecular replacement.* The structures of both drug–virus complexes were determined by molecular replacement based on the refined model of native P1/Mahoney. To reduce the effects of model bias, residues associated with significant difference electron-density features (Fig. 3), solvent, and bound ligands all were removed from the P1/Mahoney atomic model. For the R80633 complex the 11 residues omitted were: Ser1097, Lys1101, Asp1102, Lys1103, Leu1104, Tyr1159, Ser1233, Asn1235, Asp1236, Phe1237 and His1248. For the R77975 complex the six residues omitted were Tyr1112, Met1132, His1149, Asp1236, Phe1237 and His3097. The phases were refined by the application of 30-fold NCS constraints to the data. After convergence of the NCS-based phase refinement, the icosahedrally averaged ‘unbiased’ map was readily interpretable both for the drug and the protein. In each structure, the drug and the altered loops of VP1 were easily modeled to fit the averaged  $F_o$  electron-density map (Fig. 5).

3.1.4. *Model and phase refinement.* After the initial round of manual building, the model was refined as described by Jacobson, Hogle & Filman (Jacobson *et al.*, 1996). NCS-based phase refinement then was reinitiated with the new model. Refinement of the phases and refinement of the model were alternated until convergence.

Throughout the NCS-based procedure, the non-crystallographic  $R$  factor and correlation coefficient were

Table 2. *Statistics for the refined atomic models*

	R80633	R77975
Non-H protein atoms	6661	6661
Non-H drug atoms	29	27
$R_{\text{cryst}}^*$	0.241	0.249
Bond lengths (r.m.s) (Å)	0.012	0.012
Bond angles (r.m.s) (°)	2.5	2.5
Variable torsions (r.m.s) (°)	26.1	26.0
Fixed dihedral angles (r.m.s) (°)	1.2	1.2

\*  $R_{\text{cryst}} = \sum_h |F_{\text{obsd}}(h) - F_{\text{calc}}(h)| / \sum_h |F_{\text{obsd}}(h)|$  where  $F_{\text{obsd}}$  and  $F_{\text{calc}}$  represent observed and model-based structure-factor magnitudes, respectively.

evaluated to determine how well the Fourier transform of the averaged map agreed with the observed structure-factor magnitudes. In the resolution range 30–2.9 Å, the final statistics were 17.49% and 0.9378, respectively, for the R80633 complex, and 18.85% and 0.9265 for the R77975 complex. In the last round of model refinement, the occupancy of the drug was estimated to be 80 and 90%, for R80633 and R77975 complexes, respectively. Individual isotropic temperature factors were included in the final atomic models whose statistics are listed in Table 2. After refinement, the fit of the atomic models to the averaged  $F_o$  maps was quite convincing (Fig. 5).

### 3.2. Structural changes

3.2.1. *Changes near the bound drug.* In the drug-binding pocket of the R80633 complex, the difference electron-density map (Fig. 3a) shows continuous positive density features all along the length of the drug. (In the drug-binding pocket, the difference map for the R77975 complex is qualitatively similar.) Variations in the thickness of the tube of density clearly indicate the orientation of the bound drug molecule.

Among the key residues making critical contacts with the drug molecules are Tyr1159, which is located near the buried end of the pocket, and Met1132, which is located near the middle. Paired positive and negative density features are associated with both of these side chains in the difference Fourier map, indicating that drug binding has caused them to shift.

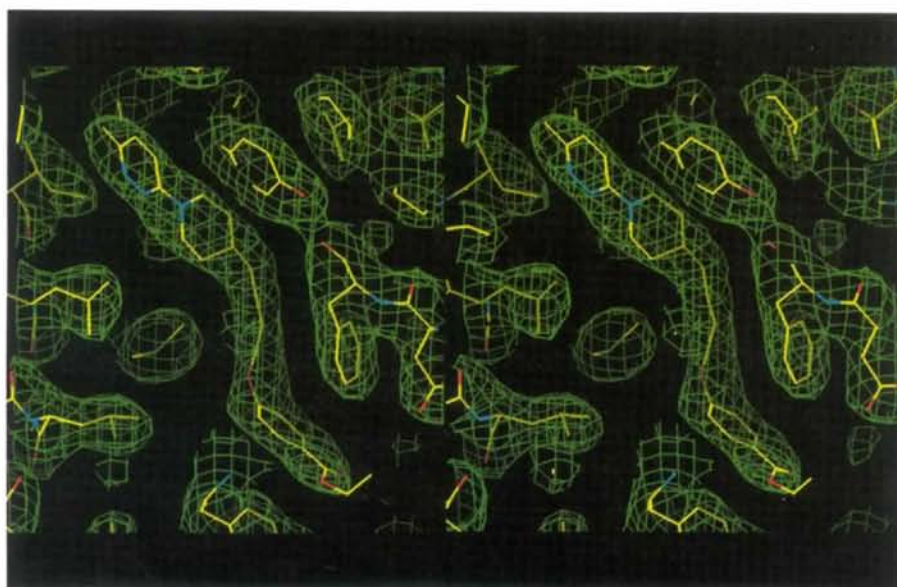
In the R80633 complex, and to a lesser extent in the R77975 complex, residues 1232–1235, at the carboxyl end of the *GH* loop of VP1, are noticeably rearranged. The main chain is shifted by about 0.5 Å. Corresponding to this, the difference map (Fig. 3a) shows strong positive difference density associated with residues 1232–1235 and with the main-chain N atom of Phe1237. In addition, paired positive and negative density features are associated with the side chains of Asn1235, Asp1236 and Phe1237; unpaired negative density features are associated with Glu1133; and unpaired positive density is seen for Ser1233 and Leu1234. Collectively, these features indicate that displacement of the natural ligand by the bulkier drug molecules

has required a noticeable local rearrangement to prevent steric conflicts.

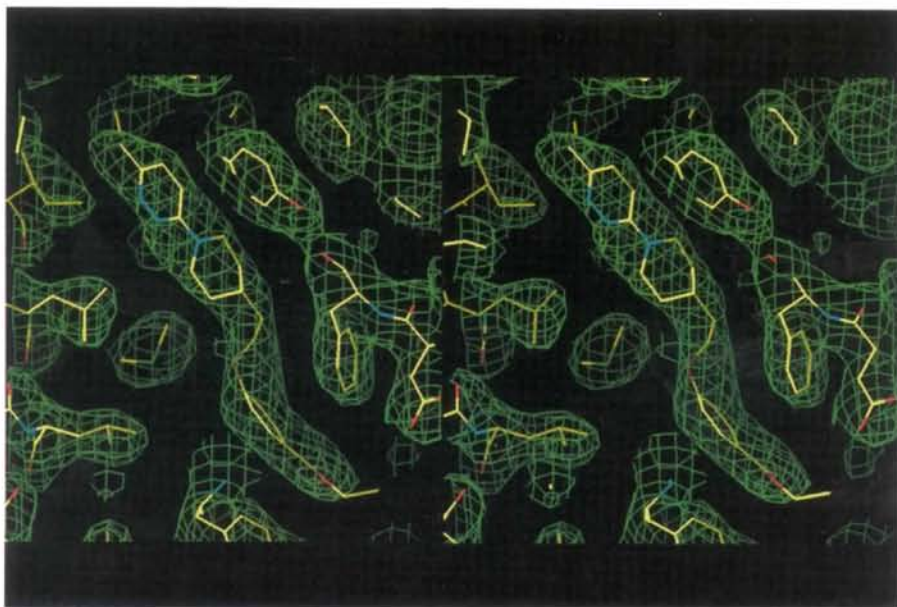
**3.2.2. Changes near the fivefold axis.** The surface of poliovirus near the fivefold axis is formed by five copies each of the *DE*, *HI* and *BC* loops of VP1 (Fig. 4). The *BC* loop is located furthest from the axis and is the most exposed. The *DE* loop is located closest to the axis, interacts extensively with other symmetry-related copies of the *DE* loop, and appears to be partially disordered in most poliovirus structures.

In the R80633 complex with P1/Mahoney, all three of these loops have moved in a concerted fashion, relative

to the native structure, shifting by as much as 0.6 Å in the *BC* and *DE* loops. This movement is indicated both by comparisons of the refined atomic models and by inspection of the difference map (Fig. 3*b*). The largest main-chain movement occurs in the portion of the *BC* loop formed by residues 1096–1102. Additional significant difference density is also associated with a cluster of side chains that includes Ser1097 and Asn1094 from the *BC* loop and His1248 from the neighboring *HI* loop. Comparably large changes in the atomic model were seen in the *DE* loop of the R77975 complex, though the difference map features were not



(a)



(b)

Fig. 5. Portions of the averaged  $F_o$  electron-density maps showing the antiviral compounds R80633 and R77975 bound to P1/Mahoney poliovirus. In these stereo representations, atoms are colored by type: C atoms are yellow, N atoms are cyan, and O atoms are red. The drug molecule extends diagonally from upper left to lower right. (a) R80633. (b) R77975. Note that the fit of both drugs to the density is quite convincing, except for the polar, outermost end of the pocket (bottom), where portions of the drug molecule are partially disordered.

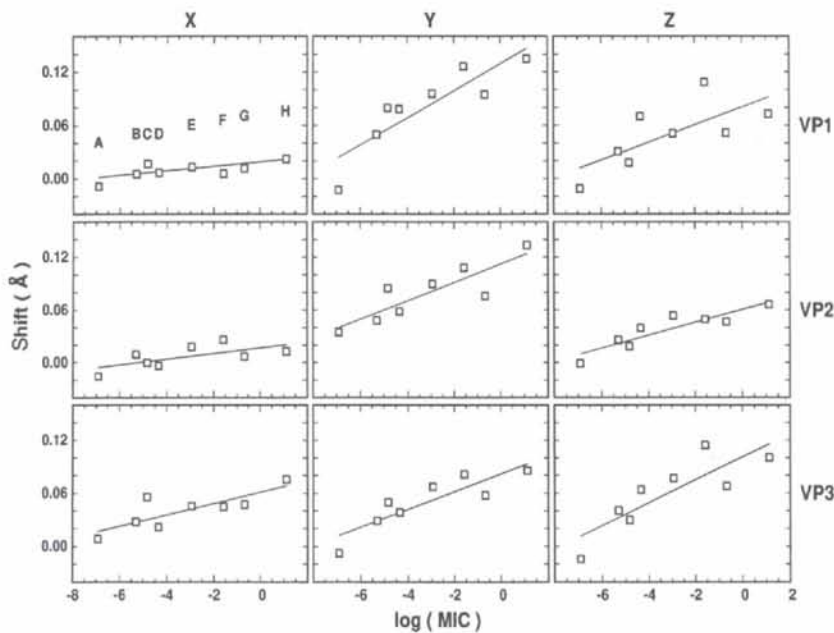


Fig. 6. Vector shifts in the major capsid proteins are correlated with drug effectiveness. Each panel in this  $3 \times 3$  array shows the shift in X, Y or Z of the center of mass of one of the major capsid proteins, VP1, VP2, or VP3, plotted as a function of drug effectiveness. The eight points in each panel represent different poliovirus–drug complexes (listed in the *Methods*). Position along the abscissa represents the natural logarithm of the minimum inhibitory concentration, the concentration of a particular drug needed to inhibit the growth of a specific virus. The position along the ordinate represents the coordinate difference between two atomic models: the drug complex minus the corresponding native structure. The data points labeled A–H in the upper left panel also serve to identify the data points in the other eight panels. The complex of R78206 with P3/242-H2 is labeled A. Complexes of P3/Sabin with R78206, R80633, WIN51711 and R77975 are labeled B, D, E and F, respectively. Complexes of P1/Mahoney with R78206, R80633 and R77975 are labeled C, G and H, respectively. Lines drawn in the plots represent least-squares fits to the data. The linear correlation coefficients ( $R_{\text{corr}}$ , for data points, the correlation between two variables  $P$  and  $Q$  is  $R_{\text{corr}} = [N\sum(PQ) - (\sum P)(\sum Q)] / ([N\sum(P^2) - (\sum P)^2][N\sum(Q^2) - (\sum Q)^2]^{1/2})$  are best for those vector components with larger slopes. Thus, for VP1, VP2, and VP3, respectively,  $R_{\text{corr}}$  values for the X component were 0.71, 0.66, and 0.81. For the Y component,  $R_{\text{corr}}$  values were 0.87, 0.86 and 0.88. For the Z component,  $R_{\text{corr}}$  values were 0.72, 0.90 and 0.84.

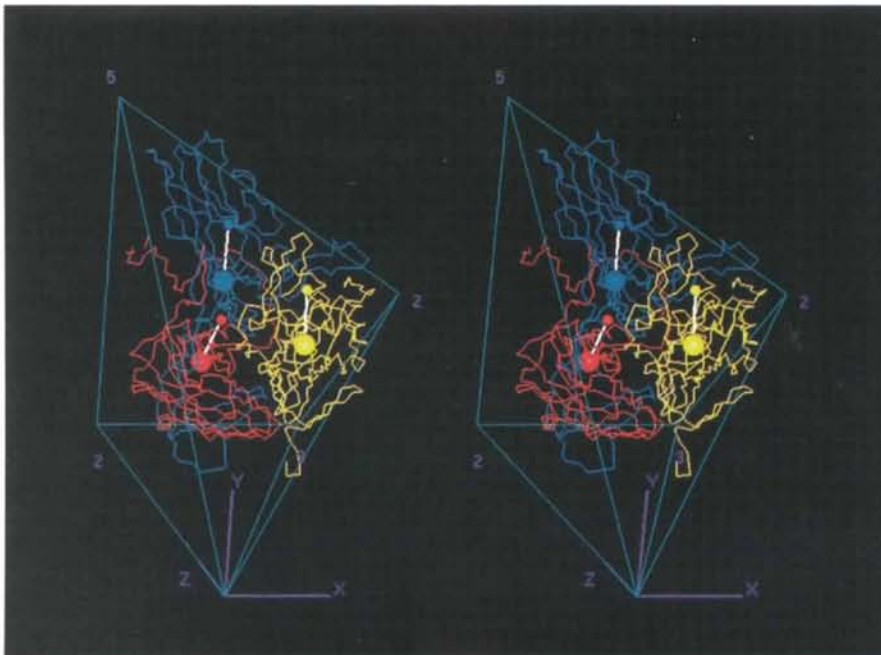


Fig. 7. Directions in which the major capsid proteins of poliovirus are shifted in response to the binding of the less effective antiviral compounds. In this stereoview,  $\alpha$  traces of the three major capsid proteins are shown superimposed on Cartesian coordinate axes (magenta) and an irregular four-sided pyramid (cyan). This pyramid represents one possible choice of the icosahedral unique volume. The edges of the pyramid include icosahedral twofold, threefold and fivefold axes which are labeled 2, 3, and 5. VP1 is blue; VP2 is yellow and VP3 is red. The large blue, yellow and red spheres represent the centers of mass of VP1, VP2, and VP3, respectively. The white rods extending from each large sphere show the direction in which each protein shifts. The length of each rod is 100 times greater than the actual shift vector.



as large at a similar level of significance. In all the poliovirus structures solved to date, a large density feature, believed to be an ion, has been found located along the particle fivefold axis, in close contact with five copies of the His1149 side chain, on the *DE* loop of VP1. In both the R80633 and R77975 complexes, this putative ion is associated with significant positive difference density, while the His1149 side chains are associated with negative difference density. Consistent with this, localized differences also are seen in the *DE* loop (residues 1142–1152) in both atomic models. Either a shift in the protein or a change in its degree of order here could produce these observed difference features. It should be noted, however, that the appearance of the electron density near the fivefold axis varies considerably among poliovirus structures, and may well be affected by experimental conditions.

### 3.3. Concerted shifts in the $\beta$ -barrels

Until the present study, no convincing structural changes were seen in poliovirus–drug complexes remote from the drug binding site. The structural changes seen here are both novel and puzzling because they are located so distant from the binding site, and because there are no obvious conformational differences in the residues intervening between the two sites to provide a mechanical explanation of how binding effects might be transmitted so far away. Consequently, an effort was made to look for concerted shifts in the coordinates of various portions of the atomic model, in hopes of seeing how the forces were transmitted. Particular attention was paid to the  $\beta$ -strands of VP1, which connect the two sites.

Statistically meaningful trends were discovered only when the major capsid proteins VP1, VP2 and VP3 were each considered as a whole. In several of the drug–virus complexes, the center of mass of each  $\beta$ -barrel was found to shift from its position in the native structure (Fig. 6). The key observation was that the shift of any particular  $\beta$ -barrel, regardless of its magnitude, generally proceeded along the same vector direction. VP1 and VP2 appear to shift most noticeably along *Y*, away from the twofold and towards the fivefold axis. In contrast, the VP3 shift has relatively large *X* and *Z* components as well, corresponding to a movement outward and tangentially around the fivefold axis (see Fig. 2 and *Methods*). These calculated shifts are reproducible, regardless of whether all of the main-chain atoms are considered, or  $C\alpha$  atoms only, or only the  $C\alpha$  atoms of the  $\beta$ -strands.

Most remarkably, the extent of these shifts are consistently correlated with the biological effectiveness of the antiviral compound. The more effective a drug is in inhibiting the growth of a particular virus, the more closely the drug–virus complex resembles the native structure. Conversely, the higher the concentration of drug required to inhibit growth of a particular virus, the more the  $\beta$ -barrels are shifted. It is worth emphasizing

that even though the total extent of the shifts is small, roughly 0.2 Å or less, the correlation of the  $\beta$ -barrel shifts with biological activity is strikingly good. Correlation coefficients (reported in Fig. 6) are statistically significant, and the best-fit lines drawn on the plots are quite convincing, even though there is no *a priori* reason to expect the relationships to be linear.

It is worth emphasizing that these results are unlikely to have been caused, trivially, by differences in experimental protocols. The virus used in all of the drug-binding studies was grown, purified, and crystallized using identical protocols. Several poliovirus variant structures that were determined contemporaneously, using the same protocols, show no similar changes in  $\beta$ -barrel location. Statistics for two such variants are provided as controls, below. Furthermore, although DMSO was used to solubilize the drugs, the levels of DMSO in this study were well within the range of DMSO concentrations used in prior studies.

### 3.4. Validity of shift calculations

Given the small size of the shifts, 0.2 Å or less, the reliability of the calculation is an issue that must be addressed. Even at the resolution of the structure determination, 2.9 Å, a concerted shift of roughly a third of the icosahedrally ordered material in the capsid would have a measurable effect on the observed structure-factor magnitudes, which would then be reflected in the refined coordinates of the model. Viewed in another way, if the uncertainty in each atomic position is 0.2–0.3 Å at this resolution, then the center of mass of *n* such atoms (if they were truly independent variables) would be known to the square root of *n*-fold greater precision. Here, plausible choices of *n* range from 200 to 2000, depending on whether the  $C\alpha$  atoms, the main-chain atoms, or all the atoms in a  $\beta$ -barrel are included. The observed shifts are therefore conservatively estimated to be at least one order of magnitude larger than the expected uncertainty in the center of mass.

### 3.5. Preventing scaling errors

In the present analysis, positional differences are calculated between atoms from different crystal structures. Potentially, the results of such a calculation could be skewed by systematic errors in the cell parameters. Two sorts of errors can be envisaged: an error in the ratio between the cell lengths, and an isotropic scaling error in the radius of the virus. Because of the use of icosahedral symmetry in the structure determination, the first potential source of error is not relevant. Thus, in the procedure used here to refine the atomic models (Jacobson *et al.*, 1996) each of the models was refined to fit non-crystallographic symmetry-constrained electron density associated with a single ‘standard’ protomer (see Fig. 2). The standard protomer represents the average of 30 protomers, each having a different orientation with

Table 3. *Vector shifts of the capsid proteins*

Virus structure	Vector component	Shift (Å)			Radial correction
		VP1	VP2	VP3	
(a) P1/Mahoney R77975 complex (uncorrected)	X	0.022	0.013	0.075	1.0000
	Y	0.135	0.134	0.085	
	Z	0.073	0.066	0.100	
(b) P1/Mahoney R77975 complex	X	0.001	-0.030	0.056	0.9991
	Y	0.091	0.105	0.063	
	Z	-0.030	-0.037	-0.009	
(c) V510	X	0.021	0.002	0.017	0.9989
	Y	0.028	0.021	0.018	
	Z	-0.038	0.010	0.001	
(d) VD9	X	0.005	-0.001	0.003	0.9999
	Y	-0.004	0.007	0.025	
	Z	-0.005	-0.002	0.001	
(e) 73S native empty capsids	X	-0.023	-0.048	-0.004	0.9976
	Y	0.143	0.079	0.054	
	Z	0.026	-0.035	-0.055	

respect to the axes of the unit cell. Consequently, an error in any single cell parameter would not cause atoms to be shifted in any particular direction.

On the other hand, the danger of mis-scaling the cell parameters isotropically is very real, particularly because the averaging statistics (see above) are insensitive to that kind of error. Positional differences similar in size to those reported here easily could be caused by 1 Å errors or less in 350 Å cell parameters. Fortunately, two simple tests are available to ensure that the concerted shifts seen in the drug-virus complexes are not artifacts of mis-scaling the particle radius.

First, if the results were due to uniform mis-scaling of the coordinates, then each of the *X*, *Y* and *Z* shifts would be roughly proportional to the *X*, *Y* and *Z* coordinates, respectively. To test this possibility, ratios of the form  $dX/X$ ,  $dY/Y$  and  $dZ/Z$  were calculated (data not shown). These ratios varied considerably, by orders of magnitude, amongst the *X*, *Y* and *Z* directions, and from protein to protein, indicating that they were not caused either by uniform expansion or by mis-scaling.

A second possible approach involves the deliberate uniform re-scaling of the drug complex coordinate set so as to minimize its mean-square discrepancy from the native structure. This provides a way to determine whether or not the capsid proteins have shifted along the viral surface, independent of any expansion that might have taken place. Even after this normalization (Table 3*b*), the coordinate comparison for the P1/Mahoney complex with R77975 continues to show a tendency for all three viral proteins to move toward the fivefold axis, and for VP3 to move tangentially around it.

Uniform rescaling of the coordinates also compensates for the possibility that the cell parameters might be incorrect. Cell parameters for the drug-virus complexes were all assumed identical to the corresponding native virus structures. No alternative was available because post-refinement of cell parameters on the basis of very limited data sets would not have been reliable. Based

on the data presented (Table 3*a,b*) it is apparent that the binding of certain ligands causes the major capsid proteins to shift positions along the viral surface, relative to the symmetry axes which serve as landmarks. It is strongly suspected that these shifts are associated with an expansion of the virus particle (see below). However, based on the data alone, it is impossible to tell whether the particle size has actually changed.

### 3.6. Comparisons with other poliovirus structures

After the  $\beta$ -barrel shifts in the drug complexes were noticed, additional control calculations were carried out to see how the magnitudes of the shifts compared with the level of variability between native poliovirus structures. Coordinates for the native P1/Mahoney model were compared with those of two independently determined type 1 poliovirus variants, VD9 (Jacobson, 1995) and V510 (Yeates *et al.*, 1991; Jacobson, 1995) which differ from P1/Mahoney in the sequence of the *BC* loop of VP1. Both variant structures are based on extensive, fairly complete data sets, and have independently determined cell parameters. (Here, the ratios between the cell lengths are very well determined, but their absolute scale cannot be considered reliable.)

There were several important reasons for looking for structural differences in V510 and VD9. Due to sequence differences in the *BC* loop of VP1, both V510 and VD9 show structural changes near the fivefold axis. In addition, both of these variants are less resistant than P1/Mahoney to thermally induced conformational changes, a property at least peripherally related to the mechanism of drug action. Furthermore, the natural lipids bound to the hydrophobic pockets of V510 and VD9 differ in appearance from those in P1/Mahoney. The lipids in V510 and VD9 have been modeled as palmitate and laurate, respectively (Yeates *et al.*, 1991; Jacobson, 1995), rather than as sphingosine. At the more polar open end of the pocket, these three ligands are very different, both in appearance and in the contacts they make with the capsid protein. However, at their more deeply buried ends, all three ligands include an extended hydrocarbon chain at least 12 C atoms long which binds in a very similar manner in all native poliovirus structures.

Despite these structural and phenotypic differences, the arrangement of  $\beta$ -barrels in V510 and VD9 are nearly identical to those in P1/Mahoney (Table 3*c,d*). Though the coordinate differences for both of these variants were relatively large prior to normalization (data not shown), all of the vector shifts became negligible after uniform rescaling of the coordinates. As it has turned out, the center-of-mass shifts for V510 and VD9 are primarily useful as negative controls for the drug-complex comparisons. They demonstrate that the exchange or elimination of a ten-residue surface loop causes only negligible rearrangement of the  $\beta$ -barrels, relative to the far more extensive effects of changing the drug structure

by a few atoms. Together with the structures of the most effectively inhibited drug complexes, these two controls also confirm that the arrangement of  $\beta$ -barrels is not strongly affected by differences in the structure of bound ligand, provided that steric conflicts in the pocket are avoided.

### 3.7. Comparisons with empty capsids

In poliovirus 73S empty capsids (Basavappa *et al.*, 1994) the lipid-binding pocket is apparently occupied by the same lipid or mixture of lipids as in the mature P1/Mahoney structure, but the viral RNA is not present. Since the stabilizing network of polypeptides on the inner capsid surface has not yet formed fully, the native antigenic empty capsids are very much less stable than mature virions. Like the VD9 and V510 structures, the empty capsid structure is based on an extensive, nearly complete data set, and has independently determined cell parameters.

When evaluating center-of-mass shifts for the empty capsids, relative to mature P1/Mahoney, a more limited set of atom pairs had to be used for evaluating the protein centroids. First, many of the polypeptide strands that form the internal network in mature virus are disordered in the empty capsid structure, making them unavailable for the coordinate comparisons. In addition, 35 ordered residues from the amino terminus of VP2 (before residue 2063) had to be excluded. These residues were sufficiently different from the native structure that including them in the calculation led to a spuriously large negative shift in the Z coordinate of VP2.

After normalization of the particle radius, the 73S-empty-versus-native comparison (Table 3e) has much in common with the drug-minus-native comparisons. Once the scaling errors are taken into account, the shifts along Y are very large and positive for both VP1 and VP2. It is worth noting that these shifts are slightly larger than those seen in the drug-virus complexes. This makes the native empty capsid structure the most highly altered structure in the continuum analyzed here, as well as the least stable.

## 4. Discussion

Crystal structures have been determined for a variety of drug complexes with poliovirus to assess the effects of changes in drug structure and in protein sequence. The structure/function correlates derived from these studies might be useful both for future design of additional capsid-binding drugs in this series and to probe the mechanism by which these drugs interfere with the conformational changes that are required for productive cell entry. In previous studies (Grant *et al.*, 1994; Hiremath *et al.*, 1995) differences associated with drug binding were small and occurred within the drug binding site. Those studies identified three critical amino-acid side chains, Met1132, Leu1134 and Leu1261, located close

together on one side of the drug binding pocket. Those three residues interact sterically with one another and can provide either favorable or unfavorable van der Waals contacts with the ligand, depending on which combination of amino acids and ligands are present. Those contacts play a major role in determining how efficiently the atoms of the ligand are packed into the available space, which accounts, in turn, for the measured MIC's. Indeed, sequence changes at those three key positions have been seen in drug-adapted and drug-resistant variants of poliovirus (Mosser, Sgro & Rueckert, 1994).

The present study looks at two of the drug-virus complexes that require relatively high concentrations of drug for inhibition. As seen previously, R77975 is somewhat too small for its binding site, and fails to fill the pocket completely at its most deeply buried end. This makes it the least effective of the four compounds studied in poliovirus. In contrast, R80633 is slightly too large for its binding site. This permits it to fill the buried end of the pocket nearly as effectively as R78206, the best of the drugs, but its longer linker forces it to make less-than-optimal contacts near the middle of the pocket. The non-optimal packing of both of these drugs is reflected by the appearance of the electron-density maps (Figs. 5a and 5b). Thus, at the more open end of the two binding pockets, there is an imperfect match between the shapes of the density envelopes and the conformations of the atomic models, which each represent the single best choice of a low-energy drug conformation.

The observed complexes confirm the predictions from our earlier structural studies. (Grant *et al.*, 1994). As anticipated, the presence of Leu1134 and Leu1261 in the drug-binding pocket of P1/Mahoney prevents the side chain of Met1132 from folding back away from the hydrocarbon chain of the drug. The conformation of Met1132 would have led to highly unfavorable steric conflicts, perhaps sufficient to have prevented the binding of these two drugs, except for the ability of the virus to respond to the stress mechanically, by adopting a less-than-optimal arrangement of  $\beta$ -barrels.

### 4.1. Concerted structural changes

The structures of the P1/Mahoney complexes with R80833 and R77975 differ significantly from the previous drug-virus complexes because believable structural changes are seen remote from the drug binding site, which affect the way that symmetry-related capsid proteins interact with one another. These structural differences include significant conformational changes near the fivefold axis, in the BC, HI and DE loops of capsid protein VP1. Surprisingly, the drug-induced alterations include concerted movements of the  $\beta$ -barrels across the surface of the virus, with each barrel shifting to a different extent, and in a different vector direction (Fig. 7). These shifts cannot be accounted for by a

uniform expansion of the particle or by a mis-scaling of the coordinates (Table 3*b*). Overall, the extent of the vector shifts is correlated surprisingly well with drug effectiveness (Fig. 6).

Although the cause of these concerted shifts is not entirely clear, one plausible explanation is that stresses in the vicinity of the drug binding pocket are relieved by an icosahedrally symmetric rearrangement of the protein subunits. It seems likely that the observed shifts result in a slightly expanded structure. However, uncertainties in the absolute magnitude of the cell parameters, and the procedures used here to eliminate scaling artifacts makes it impossible to verify actual swelling of the particle. Regardless of whether the particle expands, the concerted shifts themselves may contribute as proximate causes of the high MIC values. Thus, when effective drugs are bound, optimal packing in the pocket permits an optimal (native-like) interaction between capsid proteins. In contrast, when less effective drugs are bound, non-optimal packing in the pocket disrupts the ground-state interaction between capsid proteins, and thereby makes major conformational transitions (such as those associated with cell entry) more feasible.

In considering the possible significance of the concerted shifts of the capsid protein subunits, two points should be considered. First, any long-range accommodation of local stress must, by definition, follow low-energy pathways that are accessible to the virion. Second, a wide range of evidence suggests that the virion is normally programmed to undergo a number of conformational changes in a concerted and symmetric fashion (*e.g.* the structural transitions leading to the 135S and 80S particles). Therefore, it seems likely that the concerted changes seen in the drug complexes (and in the empty capsids) sample near-equilibrium steps of trajectories in the normal conformational repertoire of the virus. The observed concerted shifts could provide useful experimental correlates of ongoing computational analysis of the conformational flexibility of the virions using normal mode analysis (von Vlijmen, Hogle & Karplus, unpublished work). Finally, it is possible, though certainly not proven, that the trajectory (sampled due to the distortions induced by drug binding) is directly relevant to the experimentally observed reversible breathing of the structure when virions are exposed to physiological temperatures (Li, Yafal, Lee, Hogle & Chow, 1994), and to the much larger, irreversible, changes associated with cell entry.

This work was supported by NIH grants AI20566 and AI32480 (to JMH), and by a grant from the Keck Foundation to establish a structural biology facility in the Department of Biological Chemistry and Molecular Pharmacology at Harvard Medical School. The authors wish to thank K. Andries for the gift of R80633 and R77975, J. Green for assistance in data processing, and M. Wien for critical reading of the manuscript.

Coordinates have been deposited with the Protein Data Bank\*

\* Atomic coordinates and structure factors have been deposited with the Protein Data Bank, Brookhaven National Laboratory (Reference: IPO1, R1PO1SF and IPO2, R1PO2SF). Free copies may be obtained through The Managing Editor, International Union of Crystallography, 5 Abbey Square, Chester CH1 2HU, England (Reference: GR0690).

## References

- Andries, K., Dewindt, B., Snoeks, J., Wouters, L., Moereels, H., Lewi, P. J. & Janssen, P. A. J. (1990). *J. Virol.* **64**, 1117–1123.
- Badger, J., Minor, I., Kremer, M. J., Olivera, M. A., Smith, T. J., Griffith, J. P., Guerin, D. M. A., Krishnaswamy, S., Luo, M., Rossmann, M. G., McKinlay, M. A., Diana, G. D., Dutko, F. J., Fancher, M., Rueckert, R. R. & Heinz, B. A. (1988). *Proc. Natl Acad. Sci. USA*, **85**, 3304–3308.
- Badger, J., Minor, I., Oliveira, M. A., Smith, T. J. & Rossmann, M. G. (1989). *Proteins*, **6**, 1–19.
- Baltimore, D., Girard, M. & Darnell, J. E. (1966). *Virology*, **29**, 179–189.
- Basavappa, R., Syed, R., Flore, O., Icenogle, J. P., Filman, D. J. & Hogle, J. M. (1994). *Protein Sci.* **3**, 1651–1669.
- Bricogne, G. (1974). *Acta Cryst.* **A30**, 395–405.
- Filman, D. J., Syed, R., Chow, M., Macadam, A. J., Minor, P. D. & Hogle, J. M. (1989). *EMBO J.* **8**, 1567–1579.
- Flore, O., Fricks, C. E., Filman, D. J. & Hogle, J. M. (1990). *Semin. Virol.* **1**, 429–438.
- Fricks, C. E. & Hogle, J. M. (1990). *J. Virol.* **64**, 1934–1945.
- Grant, R. A., Hiremath, C., Filman, D. J., Syed, R., Andries, K. & Hogle, J. M. (1994). *Curr. Biol.* **4**, 784–797.
- Hiremath, C. N., Grant, R. A., Filman, D. J. & Hogle, J. M. (1995). *Acta Cryst.* **D51**, 473–489.
- Hogle, J. M., Chow, M. & Filman, D. J. (1985). *Science*, **229**, 1358–1365.
- Jacobson, D. H. (1995). PhD thesis, University of California, San Diego, CA, USA.
- Jacobson, D. H., Hogle, J. M. & Filman, D. J. (1996). *Acta Cryst.* **D52**, 693–711.
- Jones, T. A. (1978). *J. Appl. Cryst.* **11**, 268–272.
- Kim, K. H., Willingmann, P., Gong, Z. X., Kremer, M. J., Chapman, M. S., Minor, I., Oliveira, M. A., Rossmann, M. G., Andries, K., Diana, G. D., Dutko, F. J., McKinlay, M. A. & Pevear, D. C. (1993). *J. Mol. Biol.* **230**, 206–227.
- Kim, S., Smith, T. J., Chapman, M. S., Rossmann, M. G., Pevear, D. C., Dutko, F. J., Felock, P. J., Diana, G. D. & McKinlay, M. A. (1989). *J. Mol. Biol.* **210**, 91–111.
- Li, Q., Yafal, A. G., Lee, Y. M.-H., Hogle, J. & Chow, M. (1994). *J. Virol.* **68**, 3965–3970.
- McSharry, J. J., Caliguiri, L. A. & Eggers, H. J. (1979). *Virology*, **97**, 307–315.
- Mosser, A. G., Sgro, J.-Y. & Rueckert, R. R. (1994). *J. Virol.* **68**, 8193–8201.
- Muckelbauer, J. K., Kremer, M., Minor, I., Diana, G., Dutko, F. J., Groarke, J., Pevear, D. C. & Rossmann, M. G. (1995). *Structure*, **3**, 653–667.
- Oliveira, M. A., Zhao, R., Lee, W.-M., Kremer, M. J., Minor, I., Rueckert, R. R., Diana, G. D., Pevear, D. C., Dutko, F. J., McKinlay, M. A. & Rossmann, M. G. (1993). *Structure*, **1**, 51–68.

- Racaniello, V. R. & Baltimore, D. (1981). *Science*, **214**, 916-919.
- Roizman, B., Mayer, M. M. & Roane, P. R. (1959). *J. Immunol.* **82**, 19-25.
- Smith, T. J., Kremer, M. J., Luo, M., Vriend, G., Arnold, E., Kamer, G., Rossmann, M. G., McKinlay, M. A., Diana, G. D. & Otto, M. J. (1986). *Science*, **233**, 1286-1293.
- Smyth, M., Tate, J., Hoey, E., Lyons, C., Martin, S. & Stuart, D. (1995). *Nature Struct. Biol.* **2**, 224-231.
- Winkler, F. K., Schutt, C. E. & Harrison, S. C. (1979). *Acta Cryst.* **35**, 901-911.
- Yeates, T. O., Jacobson, D. H., Martin, A., Wychowski, C., Girard, M., Filman, D. J. & Hogle, J. M. (1991). *EMBO J.* **10**, 2331-2341.